PNAS RESEARCH ARTICLE | NEUROSCIENCE

Parkinson's-linked LRRK2-G2019S derails AMPAR trafficking, mobility, and composition in striatum with cell-type and subunit specificity

Swati Gupta[a,b], Alexander Tielemans[a,b,c], Christopher A. Guevara[a,b,c], George W. Huntley[a,b,c,1], and Deanna L. Benson[a,b,c,1]

Affiliations are included on p. 8.

Edited by Christine M. Gall, University of California at Irvine, Irvine, CA; received October 22, 2023; accepted May 27, 2024 by Editorial Board Member Carol A. Mason

Parkinson's disease (PD) is a multifactorial disease that affects multiple brain systems and circuits. While defined by motor symptoms caused by degeneration of brainstem dopamine neurons, debilitating non-motor abnormalities in fronto-striatal-based cognitive function are common, appear early, and are initially independent of dopamine. Young adult mice expressing the PD-associated G2019S missense mutation in *Lrrk2* also exhibit deficits in fronto-striatal-based cognitive tasks. In mice and humans, cognitive functions require dynamic adjustments in glutamatergic synapse strength through cell-surface trafficking of α-amino-3-hydroxy-5-methyl-4-isoxazolepropionic acid-type glutamate receptors (AMPARs), but it is unknown how LRRK2 mutation impacts dynamic features of AMPAR trafficking in striatal projection neurons (SPNs). Here, we used *Lrrk2*^{G2019S} knockin mice to show that surface AMPAR subunit stoichiometry is altered biochemically and functionally in mutant SPNs in dorsomedial striatum to favor the incorporation of GluA1 over GluA2. GluA1-containing AMPARs were resistant to internalization from the cell surface, leaving an excessive accumulation of GluA1 on the surface within and outside synapses. This negatively impacted trafficking dynamics that normally support synapse strengthening, as GluA1-containing AMPARs failed to increase at synapses in response to a potentiating stimulus and showed significantly reduced surface mobility. Surface GluA2-containing AMPARs were expressed at normal levels in synapses, indicating subunit-selective impairment. Abnormal surface accumulation of GluA1 was independent of PKA activity and was limited to D_1R SPNs. Since LRRK2 mutation is thought to be part of a common PD pathogenic pathway, our data suggest that sustained, striatal cell-type specific changes in AMPAR composition and trafficking contribute to cognitive or other impairments associated with PD.

endocytosis | receptor mobility | GluA1 | LTP | direct-pathway SPN

Leucine-rich repeat kinase 2 (LRRK2), a multifunctional kinase, has been the subject of intense study since it was discovered that inherited, autosomal dominant mutations that increase its kinase activity also increase risk for Parkinson's disease (PD). Elevated LRRK2 levels or kinase activity, in the absence of mutation, also occur in patients with idiopathic PD (1, 2), suggesting that the enzyme is part of a common disease pathology. Fronto-striatal-based cognitive symptoms and altered corticostriatal processing can appear early in PD, prior to motor symptoms that are caused by the loss of dopamine neurons in the substantia nigra (3). Mechanisms driving such early symptoms and signatures are unknown, and there are no effective therapies to halt or reverse cognitive symptoms of PD.

LRRK2 expression levels are very low in dopamine neurons but enriched in striatal projection neurons (SPNs). SPNs are obligatory processing units within looped brain circuits important for initiating or terminating action sequences that underlie goal-directed and habitual responses. SPNs receive the vast majority of their input from neocortical glutamatergic pyramidal cells and their outflow takes a direct or indirect path to the substantia nigra based on cellular identity defined principally by expression of either *Drd1* (encoding dopamine receptor D_1R, direct-pathway SPNs) or *Drd2* (encoding D_2R, indirect-pathway SPNs) (4). Lasting bidirectional changes in strength of glutamatergic synapses onto both SPN subtypes are thought to encode striatal-based learning and consistent with this idea, glutamatergic synapses in D_1R and D_2R SPNs undergo persistent strengthening (long term potentiation, LTP) and weakening (long term depression, LTD) (5–8). Previous work shows that in mice expressing a PD-associated *Lrrk2*^{G2019S} mutation, LTP is abolished in both SPN subtypes in dorsomedial striatum, abrogating normal bidirectional synaptic plasticity required for striatal function (9, 10). As may be predicted

Significance

Mutations in LRRK2 are common genetic risks for Parkinson's disease. *Lrrk2*^{G2019S} mice fail to exhibit long-term potentiation at corticostriatal synapses and show significant deficits in frontal-striatal-based cognitive tasks. While LRRK2 has been implicated generally in protein trafficking, whether G2019S alters AMPAR trafficking at synapses on striatal projection neurons (SPNs) is unknown. We show that surface GluA1-AMPARs fail to internalize and accumulate excessively within and outside synapses. This effect is selective to D_1R SPNs and negatively impacts synapse strengthening as GluA1-AMPARs fail to increase at synapses in response to potentiation and show limited surface mobility. Thus, LRRK2-G2019S narrows the effective range of plasticity mechanisms, supporting the idea that cognitive symptoms reflect an imbalance in AMPAR trafficking mechanisms within cell-type-specific projections.

Author contributions: S.G., A.T., C.A.G., G.W.H., and D.L.B. designed research; S.G., A.T., and C.A.G. performed research; S.G., A.T., C.A.G., and D.L.B. analyzed data; and S.G., G.W.H., and D.L.B. wrote the paper.

The authors declare no competing interest.

This article is a PNAS Direct Submission. C.M.G. is a guest editor invited by the Editorial Board.

[1]To whom correspondence may be addressed. Email: george.huntley@mssm.edu or deanna.benson@mssm.edu.

This article contains supporting information online at https://www.pnas.org/lookup/suppl/doi:10.1073/pnas.2317833121/-/DCSupplemental.

Published July 5, 2024.

by this more restricted synapse plasticity range, *Lrrk2*^{G2019S} mice exhibit significant dysfunction in striatally based goal-directed learning and visuospatial attention tasks (11) that bear similarities to cognitive domains impaired in PD (3, 12–14).

Based in part on work in other cell types, both the impairment in cognitive tasks that require striatal synapse plasticity coupled with abnormal synaptic plasticity in *Lrrk2*^{G2019S} SPNs has raised the possibility of defects in cellular mechanisms that target and regulate AMPA-type glutamate receptor (AMPAR) trafficking dynamics at striatal glutamatergic synapses (9, 15). Here, we test this directly. The data show that there is a SPN subtype- and AMPAR subunit-specific impact of *Lrrk2*^{G2019S} on AMPAR trafficking that serves to increase receptor stability on the surface at synaptic and nonsynaptic sites. This has a profound impact on AMPAR subunit composition. Since AMPARs mediate most excitatory activity in the brain, the data suggest that a sustained increase in LRRK2 kinase activity broadly impacts information flow relevant to depression, anxiety, and cognitive symptoms of early PD.

Results

Surface Pool of GluA1-Containing AMPARs Is Increased in *Lrrk2*^{G2019S} SPNs. Previous work has shown that AMPAR-mediated activity is decreased in *Lrrk2* knockout SPNs while amplitude of AMPAR-mediated currents is increased in *Lrrk2*^{G2019S} SPNs during the first weeks of postnatal development (16, 17). Based on these findings, we first asked whether AMPAR synthesis in striatal cells was altered in mice carrying a knockin mutation of *Lrrk2*^{G2019S} (16). We used bulk RNAseq to compare expression of AMPAR subunit mRNAs in *Lrrk2*^{G2019S} and wildtype (WT) mouse striata at P21 (GSE246117) (18). A volcano plot revealed that the mutation had a limited impact on transcription overall (*SI Appendix*, Fig. S1*A*) and there were no significant differences in levels of mRNAs encoding AMPAR subunits GluA1–4 (*SI Appendix*, Fig. S1*B*). Comparisons of AMPAR subunit transcript levels between patient-derived *LRRK2*^{G2019S} iPSCs and isogenic controls (GSE183499) (19) and between putamen isolated from human PD patients and age-matched controls (GSE136666) (20) also showed no *LRRK2*^{G2019S}-dependent or PD-associated differences in levels of AMPAR subunit mRNAs (*SI Appendix*, Fig. S1*B*). The absence of an effect of *Lrrk2*^{G2019S} on AMPAR transcription in striatum is also consistent with previous data showing that total levels of GluA1 and GluA2 proteins are similar in striatal lysates from *Lrrk2*^{G2019S} and WT mice (9, 15).

We next asked whether *Lrrk2*^{G2019S} regulates AMPAR subunit distribution between internal (i) and cell surface (s) receptor pools. To do this, we measured sGluA1 and sGluA2 levels in dissociated corticostriatal cocultures in which we first labeled for AMPARs and then mildly permeabilized the cells to label for DARPP-32, a cytoplasmic protein that fills SPNs (Fig. 1*A*), but not other striatal cell types, and postsynaptic density marker PSD95. Tau-STED (stimulation emission depletion microscopy), a superresolution approach (21), was used to capture sGluA subunits. Total area and intensity of sGluA1 clusters within PSDs were significantly greater in *Lrrk2*^{G2019S} SPN postsynapses compared to wild type (Fig. 1 *B* and *C*). In contrast, total area of sGluA2 clusters within PSDs was similar between genotypes, but sGluA2 intensity was diminished at *Lrrk2*^{G2019S} PSDs compared to wild type, suggesting a modest

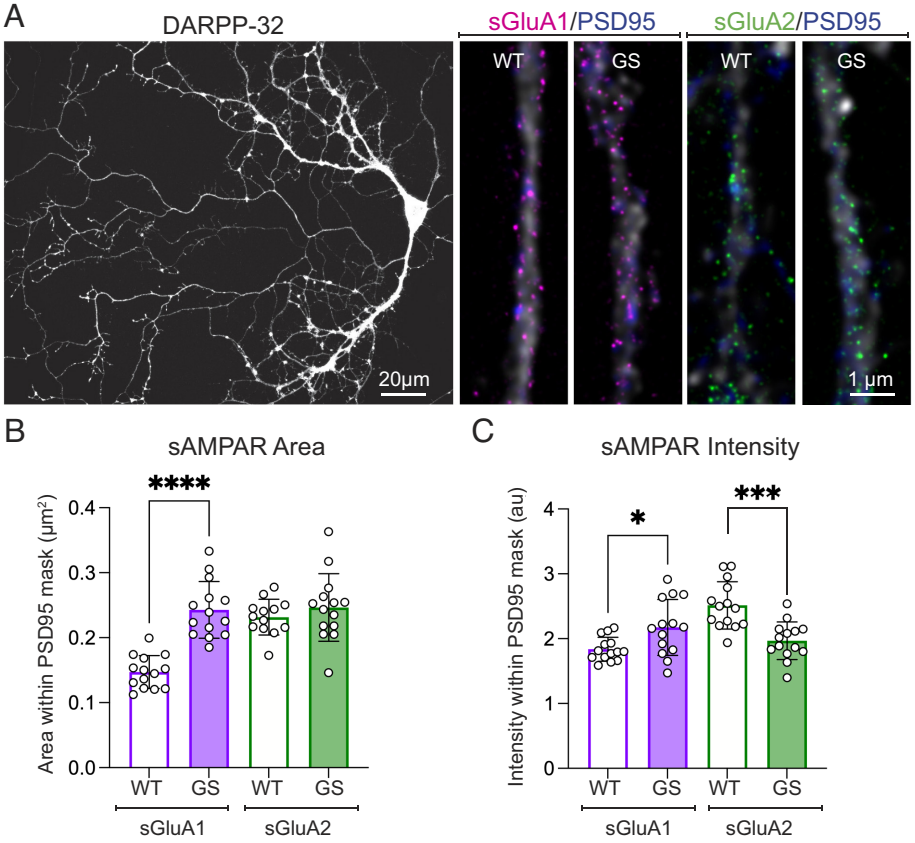

Fig. 1. *Lrrk2*^{G2019S} disrupts AMPAR stoichiometry and subsynaptic distribution in SPNs. (*A*) Confocal image of DARPP32-labeled (white) cocultured SPN (*Left*) and confocal + superresolution, STED images (*Right*) of dendritic processes. Punctate sGluA1 (magenta), sGluA2 (green) labeling (tagged prior to permeabilization) associates largely but not completely with PSD95 labeling (blue). (*B* and *C*) Bar and scatterplots compare surface AMPAR area (*B*) and intensity (*C*) within masks defined by PSD95 labeling in SPNs. Unpaired *t* test, ****$P < 0.0001$; ***$P = 0.0002$; *$P = 0.0125$. n = 14 neurons per group sampled equally from three preparations. GS, *Lrrk2*^{G2019S}; WT, wildtype.

reduction in sGluA2-containing AMPARs at postsynapses (Fig. 1 *B* and *C*). To confirm that our results in cultured neurons reflected striatal neurons in vivo, we covalently tagged all cell-surface proteins with a reactive biotin-ester in acute striatal slices from *Lrrk2*^{G2019S} and WT mice, extracted the biotinylated proteins from lysates using streptavidin coated beads and identified AMPAR subunits by western blotting. These data confirm that sGluA1 levels, but not sGluA2 levels, were elevated significantly in *Lrrk2*^{G2019S} striatum compared to WT (*SI Appendix*, Fig. S2).

Endocytosis of GluA1-Containing AMPARs Is Greatly Impeded in *Lrrk2*^{G2019S} SPNs. Increased levels of sGluA1-containing AMPARs could reflect impaired constitutive endocytosis. To probe this, we tracked and compared the extent of endogenous sGluA1 internalization in *Lrrk2*^{G2019S} and WT SPNs using an antibody feeding assay (Fig. 2*A*). A direct-conjugated, ATTO 594-tagged GluA1 rabbit polyclonal antibody (red) was used to label sGluA1 in SPNs that were cooled to prevent endocytosis and then fixed (t_0) or chased at 37 °C for 60 min (t_{60}), when AMPAR subunit internalization has plateaued (22, 23). All tagged sGluA1 was then labeled with anti-rabbit Alexa 647 (green) after which neurons were mildly permeabilized to label for DARPP-32 (Fig. 2 *B* and *C*). In WT SPNs at t_0, intensity profiles along lines drawn through individual clusters show nearly complete overlap between red and green surface signals but by t_{60}, are dominated by internalized (red-only) signal (Fig. 2*D* vs. 2*E*), as expected. In contrast, intensity profiles in *Lrrk2*^{G2019S} dendrites appear similar at t_0 and t_{60} (Fig. 2*F* vs. 2*G*), suggesting that sGluA1 failed to internalize over time. To compare internalization across time and genotype, we measured the intensity of both fluorophores and generated an internalization index defined as the percent change in the ratio of surface/total GluA1 intensity (Fig. 2*H*). At t_0, the mean internalization index value is near zero for both genotypes, but the value declines significantly at t_{60} as expected in WT SPNs. In contrast, the internalization index remains virtually unchanged in *Lrrk2*^{G2019S} SPNs between t_0 and t_{60}. These data show that in *Lrrk2*^{G2019S} SPNs, GluA1-containing AMPARs failed to internalize. Since AMPARs are internalized by clathrin-mediated endocytosis (CME) (22, 24, 25), we tested whether CME was generally deficient in *Lrrk2*^{G2019S} SPNs by assaying transferrin receptor internalization (a marker for this pathway). However, transferrin receptors were internalized normally and similarly between genotypes (*SI Appendix*, Fig. S3), suggesting the impact of *Lrrk2*^{G2019S} on the internalization of surface receptors is selective.

An LTP Stimulus Fails to Increase sGluA1-Containing AMPARs at *Lrrk2*^{G2019S} SPN Synapses Despite Intact PKA-Mediated GluA1-S845 Phosphorylation. LTP of corticostriatal synaptic strength in SPNs may involve rapid insertion of calcium-permeable (CP) AMPAR subunits such as GluA1 (26), similar to hippocampal CA1 pyramidal neurons (27). The elevated accumulation of surface GluA1-containing AMPARs in *Lrrk2*^{G2019S} SPNs suggests that the inability to express corticostriatal LTP (9) may reflect GluA1 saturation, preventing the recruitment or insertion of additional GluA1-containing AMPARs needed to increase synapse strength. To examine this, we asked whether we could drive an increase in surface AMPAR subunits in *Lrrk2*^{G2019S} SPNs using a chemical-LTP (cLTP) stimulus applied to corticostriatal cocultures (28). LTP in SPNs is mechanistically similar to PKA-dependent LTP in hippocampus in which CP-AMPARs (those lacking edited GluA2) are newly recruited to postsynaptic membranes within 5 min following induction (6, 27, 29, 30). Five minutes following cLTP stimulation, cell surface proteins were biotinylated, isolated, and probed for GluA1 and GluA2 by western blot (Fig. 3*A*). In WT neurons, cLTP increased sGluA1 levels significantly compared to ACSF controls and the effect was blocked by the

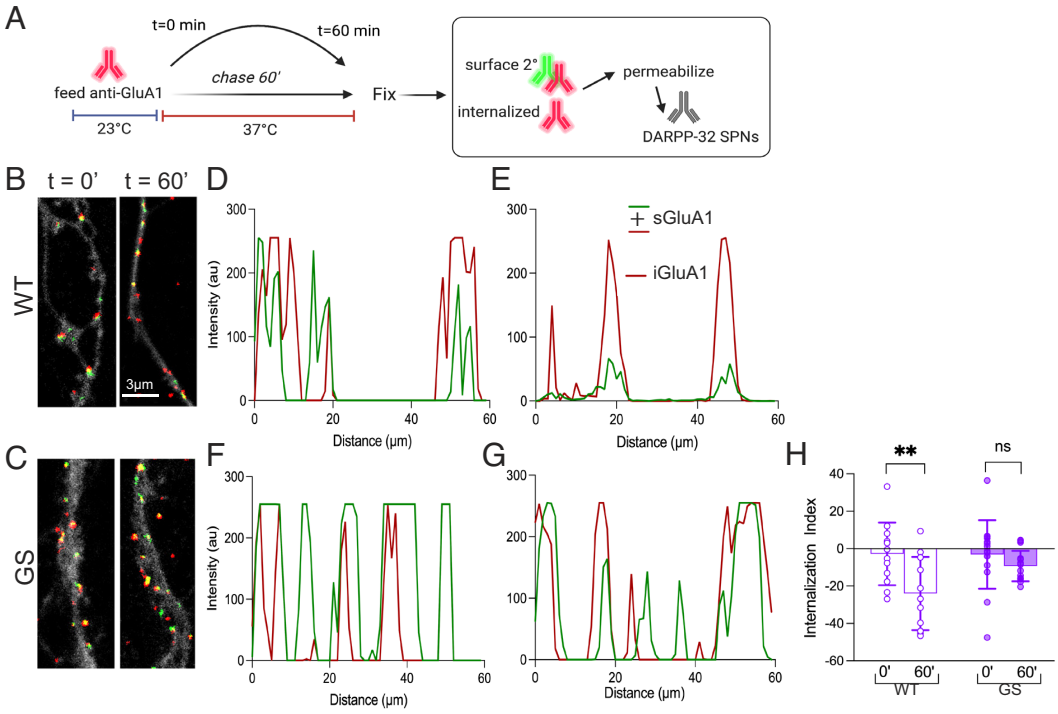

Fig. 2. *Lrrk2*^{G2019S} disrupts GluA1 internalization in SPNs. (*A*) Schematic illustrates antibody feeding assay used to monitor GluA1 internalization in WT and *Lrrk2*^{G2019S} (GS) corticostriatal cocultures (DIV16–18) and also serves as a key for the colors used to show data. (*B* and *C*) Overlay images show labeled surface (s) GluA1 (green mask + red mask) and internalized (i) GluA1 (red mask only) signal contained within DARPP-32 labeled SPNs (shown at a reduced intensity to permit visualization of puncta. Masks were generated in Image J and magnification is shown in (*B*). (*D*–*G*) Intensity distribution of green and red labeling along a 60 µm line scan. (*H*) Quantification of the internalization index of GluA1 receptors in WT and GS SPNs at 0 and 60 min (n = 12 to 16 cells, three preps/genotype, mean ± SD). Two-way ANOVA [F (1, 50) = 9.809, *P* = 0.0029], post hoc Šidák test ***P* = 0.0049.

N-methyl-D-aspartate (NMDA)-R inhibitor APV, as expected (Fig. 3 *B* and *C*). In contrast, *Lrrk2*^{G2019S} neurons failed to increase sGluA1 levels in response to cLTP treatment compared to ACSF treatment, while exposure to APV produced slightly, but not significantly, lower levels of sGluA1 compared to ACSF controls (Fig. 3 *B* and *C*). There were no differences in sGluA2 levels across treatments (Fig. 3 *C* and *D*). To confirm that the data from mixed cultures reflect SPNs, we measured and compared surface immunolabeling for GluA1 and GluA2 in DARPP-32-identified wild type and *Lrrk2*^{G2019S} SPNs (Fig. 3 *E–H*). These data matched the biochemical findings: There was a significant, NMDAR-dependent increase in sGluA1 levels in WT SPNs 5 min after cLTP, but this effect was absent in *Lrrk2*^{G2019S} SPNs (Fig. 3 *E* and *G*), while sGluA2 levels were unchanged across genotypes or treatment conditions (Fig. 3 *F* and *H*).

Following LTP induction, GluA2-lacking AMPARs are replaced by GluA2-containing AMPARs after 30 min (27, 31). Thus, to determine whether *Lrrk2*^{G2019S} also affected activity-dependent trafficking of GluA2-containing AMPARs, we compared sGluA2 levels in WT and *Lrrk2*^{G2019S} SPNs 30 min following cLTP stimulation (Fig. 3*A*). In WT SPNs, sGluA2 levels were increased significantly at 30 min compared to ACSF controls (Fig. 3*J*), while GluA1 levels had returned to control values (Fig. 3*I*), consistent with a receptor swap as expected. Increased sGluA2 levels 30 min post-cLTP were blocked by APV treatment (Fig. 3*J*). In contrast, *Lrrk2*^{G2019S} SPNs showed a significant *decrease* in sGluA2 levels 30 mins following cLTP—an effect that was blocked by APV (Fig. 3*J*), and there were no differences in sGluA1 levels between 5 and 30 min post-cLTP treatment (Fig. 3*I*).

PKA-mediated GluA1-S845 phosphorylation (pGluA1-S845) can drive AMPAR subunit insertion into the plasma membrane

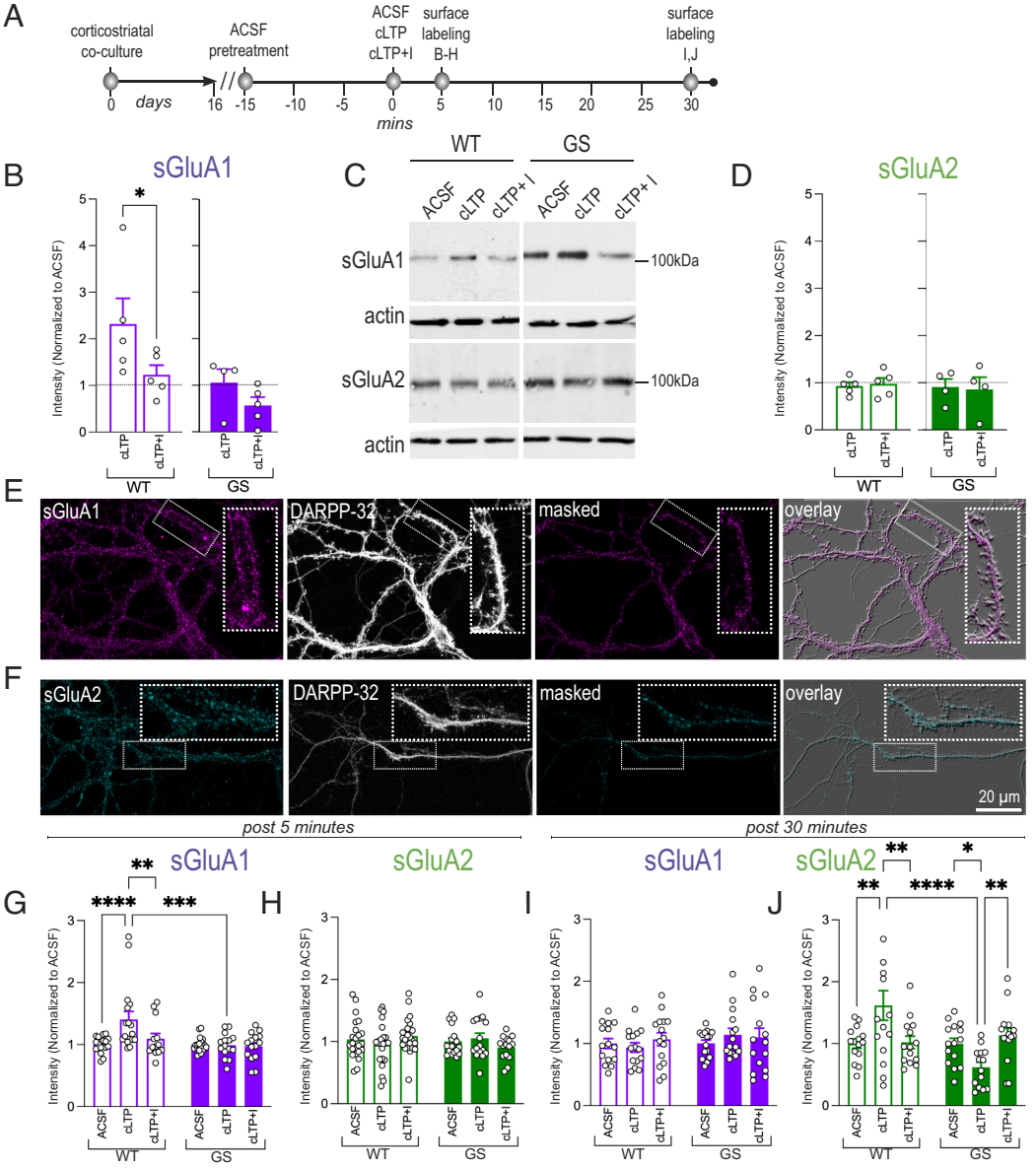

Fig. 3. Surface GluA1-AMPAR levels fail to increase in response to cLTP in *Lrrk2*^{G2019S} SPNs. (*A*) Schematic depicting experimental design. (*B–D*) Representative western blot data (*C*) and scatterplot/bar graph showing quantification of biotinylated sGluA1 (*B*) and sGluA2 (*D*) in WT and GS cocultures in response to cLTP or cLTP + I (NMDA antagonist, APV) normalized to ACSF controls (dotted lines) ± SEM. One-way ANOVA, [F (5, 23) = 4.661, *P* = 0.0044], post hoc Šidák's test: ***P* = 0.0097, **P* = 0.039. (n = 4 to 5 preps/genotype). (*E* and *F*) Confocal images of cocultured WT and GS SPNs, immunolabeled for DARPP-32 (white, *E* and*F*), sGluA1 (magenta, *E*), or sGluA2 (cyan, *F*), following treatment with ACSF, cLTP, or cLTP+I. (*G–J*) Scatterplot/bar graphs show intensity levels (normalized to ACSF control for each group ± SEM) of sGluA1 and sGluA2 at 5 (*G* and *H*) and 30 (*I* and *J*) min posttreatment (*A*). (*G*) Mixed effects analysis F (1,38) = 9.44, *P* = 0.0039 genotype, F (2,52) = 4.26, *P* = 0.0192 treatment, and F (2,38) = 4.79, *P* = 0.0139 interaction; post hoc Fisher's, *****P* < 0.0001, ****P* = 0.0002, ***P* = 0.004; (*G* and *H*) (n = 13 to 19 cells, three preps/treatment). (*J*) Mixed effects analysis [F(1, 28) = 8.36, *P* = 0.0073, genotype; F(2, 28) = 11.65, interaction, *P* = 0.0002], post hoc Fisher's multiple comparison test, *****P* < 0.0001 ***P* = 0.002, **P* = 0.04 (*I* and *J*) (n = 13 to 15 cells, three preps/treatment).

of SPNs (32–35), although there is debate whether this is required for LTP (36). While prior work has shown that LRRK2 can bind to and regulate the localization of PKARIIß, which negatively regulates PKA activity (17, 37), the G2019S mutation does not appear to impact this interaction (15, 17). Nevertheless, given the potential relevance of PKA activity here, we tested whether PKA-mediated pGluA1-S845 was disrupted in mutant SPNs by treating acute striatal slices from wild type and *Lrrk2*^{G2019S} mice with forskolin, a potent activator of adenylyl cyclase that increases PKA activity, followed by surface biotinylation and western blotting to compare total and surface levels of pGluA1-S845. In untreated striatum, levels of pGluA1-S845 phosphorylation were negligible, with no significant differences observed between genotypes (38) (*SI Appendix*, Fig. S4 *A* and *B*). Forskolin treatment significantly and similarly increased pGluA1-S845 levels measured in the input fractions in both genotypes (*SI Appendix*, Fig. S4 *A* and *B*). Forskolin treatment also increased surface pGluA1-S845 levels significantly in WT striatum, as expected (*SI Appendix*, Fig. S4 *A* and *C*). However, forskolin treatment failed to drive a significant increase in surface pGluA1-S845 in *Lrrk2*^{G2019S} striatum (*SI Appendix*, Fig. S4 *A* and *C*). These data support that PKA activation and phosphorylation of GluA1 are intact in *Lrrk2*^{G2019S} striatum, but insertion or retention of pGluA1-S845-AMPARs in the plasmalemma is compromised.

Enriched and Highly Stabilized Pool of Synaptic CP-AMPARs in *Lrrk2*^{G2019S} D_1R SPNs. Direct-pathway (D_1R-expressing) and indirect-pathway (D_2R-expressing) SPNs drive competing circuits mediating movement, reinforcement learning, and reward. To test whether the excessive accumulation of sGluA1 in *Lrrk2*^{G2019S} SPNs is functional and to evaluate whether such impaired GluA1 trafficking dynamics showed direct/D_1R or indirect/D_2R SPN subtype specificity, we crossed *Lrrk2*^{G2019S} mice with a transgenic line expressing *Drd1*a-tdTomato (39). We used whole-cell patch clamp recordings from dorsomedial striatum in acute slices to compare the sensitivity of cortically evoked AMPAR-mediated postsynaptic currents (eEPSCs) to NASPM, a selective blocker of GluA2-lacking, CP-AMPARs (40). In WT D_1R SPNs (tdTomato-positive), NASPM decreased eEPSC amplitudes by about 40% compared to eEPSC amplitudes prior to NASPM exposure. In contrast, eEPSCs in *Lrrk2*^{G2019S} D_1R SPNs were significantly more sensitive to NASPM, decreasing eEPSC amplitudes by about 70% (Fig. 4*A*), consistent with a significant enrichment of synaptic GluA1 shown biochemically and anatomically above. The addition of GluA1-enriched, GluA2-lacking AMPARs increases inward rectification of AMPAR-mediated EPSCs at positive membrane voltages (41, 42). Analysis of the I:V curves in identified SPN subtypes (*SI Appendix*, Fig. S5 *A–C*) showed a shift toward rectification in *Lrrk2*^{G2019S} D_1R SPNs compared to wild type (Fig. 4*B*) and comparison of the rectification index (amplitude at −70/+40 mV) confirmed a significant increase in rectification of corticostriatal synapses onto D_1R SPNs in mutants (Fig. 4*C*). Additionally, we found a significantly larger AMPAR:NMDAR ratio at corticostriatal synapses onto D_1R SPNs in mutants compared to wild type (*SI Appendix*, Fig. S5 *G* and *H*), all of which is consistent with the excessive accumulation of synaptic GluA1.

In contrast to D_1R SPNs, NASPM had little effect on eEPSCs in WT or *Lrrk2*^{G2019S} putative D_2R SPNs (tdTomato-negative, Fig. 4*D*). Consistent with a lack of sensitivity to NASPM, there were no significant differences between mutant and wild type in rectification (Fig. 4 *E* and *F*), nor in AMPAR:NMDAR ratios (*SI Appendix*, Fig. S5 *D–F*, *I*, and *J*) at synapses onto D_2R SPNs. Together, these data show that the enhanced sGluA1 levels observed biochemically and anatomically in *Lrrk2*^{G2019S} SPNs are functional and that altered AMPAR subunit stoichiometry at corticostriatal synapses predominantly occurs in D_1R SPNs.

Receptor subunit nanoclusters detected using STED can be used to estimate receptor composition (28). Thus, to compare AMPAR composition between genotypes in D_1R SPNs, we used τ-STED to resolve and quantify numbers of sGluA1- and sGluA2-containing nanoclusters within PSDs in D_1R SPNs cultured from wild type or *Lrrk2*^{G2019S} mice that were identified by D_1R-Cre-dependent expression of tdTomato (Fig. 4 *G* and *H* and *Materials and Methods*). *Lrrk2*^{G2019S} D_1R SPNs exhibited greater numbers of synaptic sGluA1 nanoclusters but no difference in synaptic sGluA2 nanoclusters compared to WT D_1R SPNs (Fig. 4*I*), supporting that there is an altered stoichiometry of sAMPAR subunits at mutant D_1R SPN synapses, with an increased proportion of GluA1 and a decreased proportion of GluA2. We next asked whether sGluA1-containing AMPARs were also accumulating at extrasynaptic sites in *Lrrk2*^{G2019S} D_1R SPNs by counting nanoclusters on dendrites outside regions labeled by PSD95. Numbers of sGluA1- but not sGluA2-containing nanoclusters were also enhanced extrasynaptically in *Lrrk2*^{G2019S} D_1R SPNs (Fig. 4*J*), suggesting that GluA1 exocytosis may be intact while deficits in GluA1 endocytosis may drive surface accumulation (Fig. 2). Since increased synaptic GluA1 is often positively correlated with synapse size, we also assessed density and size of PSD95-labeled clusters in D_1R SPN dendrites, but no genotype-dependent differences were detected (*SI Appendix*, Fig. S6). These data are consistent with studies showing that the *Lrrk2*^{G2019S} mutation does not impact PSD95 area and spine size in mature D_1R SPNs (15, 44).

An increase in extrasynaptic sGluA1-containing AMPARs might serve as a resource for synaptic trafficking when conditions demand (45, 46), but the failure to rapidly recruit GluA1-containing AMPARs in *Lrrk2*^{G2019S} SPNs in response to cLTP (Fig. 3) suggests that this pool is unavailable. To compare the dynamics of sGluA1-AMPAR trafficking in D_1R-SPNs, we measured fluorescence recovery after photobleaching (FRAP) of SEP-tagged GluA1 expressed in wild type and *Lrrk2*^{G2019S} D_1R SPNs expressing td-Tomato. SEP is a pH-sensitive GFP variant that emits fluorescence at the cell surface (pH 7.4) but is quenched in the acidic environment of intracellular vesicles [<pH 6; (47)]. Repopulation of a photobleached area with SEP-GluA1 receptors results from lateral diffusion from neighboring unbleached areas and exocytosis from intracellular compartments. We photobleached 1.2-µm-diameter ROIs that were centered on the heads of dendritic spines using a 488 nm laser, and fluorescence recovery was monitored every 2.5 s for 4 min subsequently using acquisition conditions that showed stable SEP-GluA1 intensity in unbleached regions and tdTomato intensity (Fig. 4*K* and *SI Appendix*, Fig. S7 *A–D*). Plots of normalized SEP-GluA1 fluorescence over time showed that the WT recovery curve fit a nonlinear biphasic association, with a τ_{fast} = 3.74 s and τ_{slow} = 93.63 s, while the *Lrrk2*^{G2019S} recovery fit a nonlinear monophasic association with a single τ = 4.76 s, closer to the τ_{fast} seen in WT (Fig. 4*L*). SEP-GluA1 recovered to only 45.2% of baseline in *Lrrk2*^{G2019S} D_1R SPN spines in comparison to 79.6% recovery in WT D_1R SPN spines (Fig. 4 *L–N*). Based on the τ values, we extrapolated diffusion coefficients for the mobile fraction of receptors (43), which show that SEP-GluA1 AMPARs in WT D_1R SPN spines diffuse at a rate 33% faster (0.035 µm^2/s) than those in *Lrrk2*^{G2019S} D_1R SPN spines (0.026 µm^2/s) (Fig. 4*N*). Thus, the excessive surface GluA1-containing receptors in *Lrrk2*^{G2019S} D_1R SPNs show greatly diminished receptor mobility.

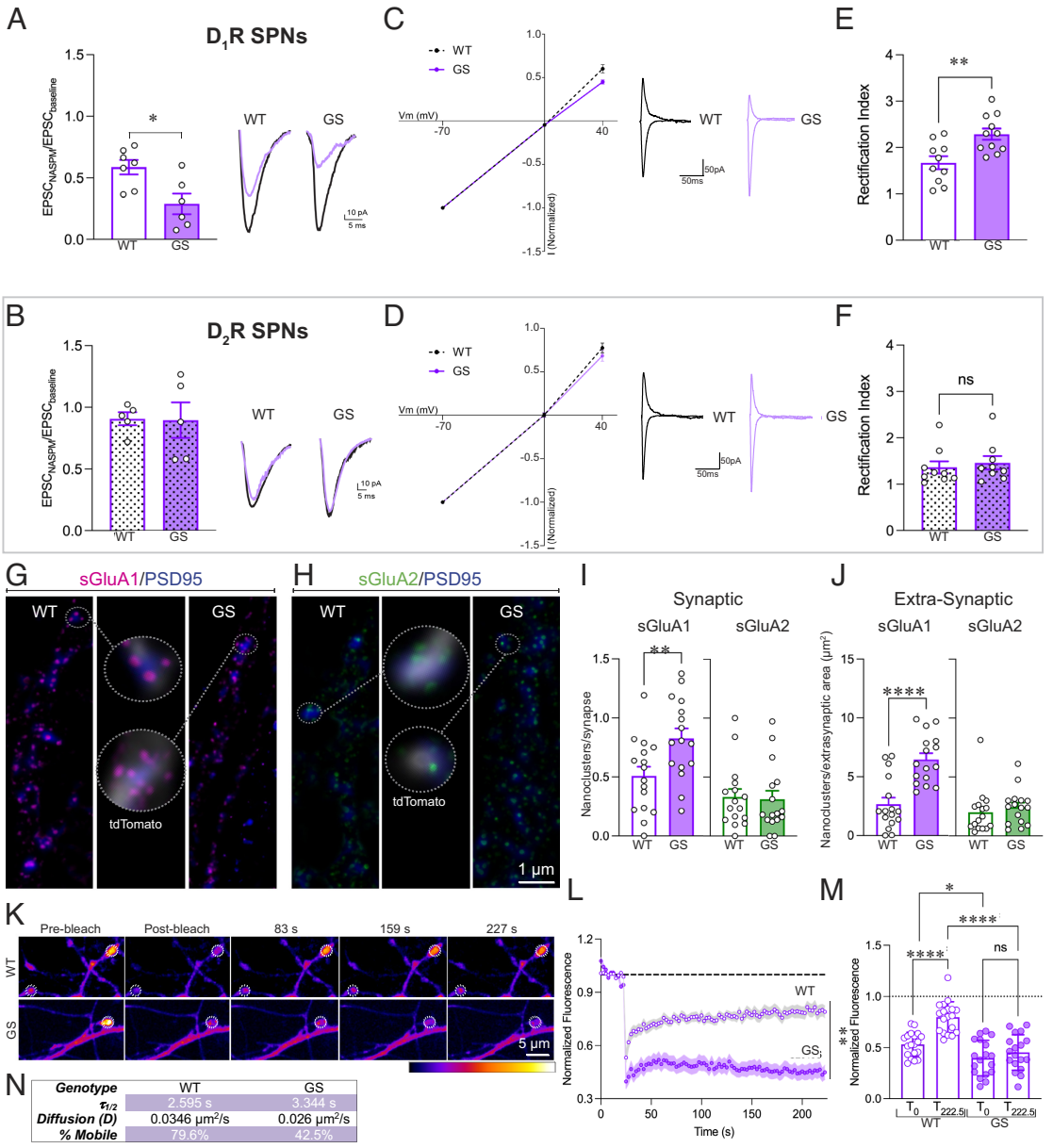

Fig. 4. *Lrrk2*^{G2019S} D_1R SPNs have an excess of stabilized CP-AMPARs. (*A* and *B*) Bar graph/scatterplots comparing functional contribution of CP-AMPARs using ratios of EPSCs evoked in the presence/absence of NASPM in D_1R (*A*; *Drd1tdTom+*) and putative D_2R (*B*; *Drd1tdTom-*) SPNs in WT and GS mice (P70–P90) in acute slices through dorsomedial striatum. Bars are mean ± SEM (n = 5 to 7 mice/group; 11 to 12 cells, unpaired *t* test **P* = 0.0122). Example traces show AMPAR currents before (black) and after (lavender) bath application of NASPM (200 µM, 10 min). (*C*–*F*) Data from dorsomedially located direct-projecting (D_1R, *B* and *E*) or indirect projecting (D_2R, *D* and *F*) SPNs in acute striatal slices identified by retrograde fluorescent bead labeling following injections into substantia nigra or GPe, respectively. (*B* and *C*) Mean AMPAR I–V relationships from wild type (WT, black dotted line) or *Lrrk2*^{G2019}(GS, purple line) SPNs (n = 3 to 4 cells/mouse, three mice/genotype/injection location). (*E* and *F*) Bar graph/scatterplots show mean rectification indices (ratio of current at −70/+40 mV) for all conditions and representative traces in the presence of APV [unpaired *t* tests, ***P* = 0.003 in (*E*) and *P* = 0.62 in (*F*)]. (*G*–*J*) Superresolution (tau-STED) images (*G* and *H*) and quantification (*I* and *J*) of synaptic and extrasynaptic receptors in 21 DIV WT and GS D_1R SPNs expressing tdTomato (white, *Drd1*Cre/+; *Ai14*, in *G* and *H*) and cocultured with unlabeled cortical neurons of the same genotype. sGluA1 (*G*, magenta, STED) and sGluA2 (*H*, green, STED) puncta in relation to PSD95 labeled postsynaptic sites (blue, confocal). Circled zones are enlarged in the center panels. (*I* and *J*) Bar graph/scatterplots show synaptic (*I*, within a mask defined by PSD95) and extrasynaptic (*J*, outside a PSD95 mask) sGluA1 (lavender) and sGluA2 (green) nanoclusters in D_1R SPNs. (*I*) Unpaired *t* test ***P* = 0.0369; (*J*) unpaired *t* test *****P* < 0.0001; n = 16 neurons/genotype. (*K*–*N*) Examples (*K*) and quantification (*L*–*N*) of FRAP experiments. (*K*) Time lapse confocal images pre- and postphotobleaching (dotted white circles approximate ROIs) in WT and GS D_1R SPNs labeled and cocultured as above. Graph (*L*) plots normalized SEP-GluA1 fluorescence recovery in WT and GS neurons imaged every 2.5 s. Lighter shading is ± SEM. Two-way RM-ANOVA [F (89, 3115) = 17.79, ***P* < 0.001], n = 18 to 19 spines/genotype. Bar graph/scatterplot (*M*) compares recovery of SEP-GluA1 intensity at T = 222.5 s time point relative to postbleach in WT and GS D_1R SPNs (mean ± SD). Two-way ANOVA [interaction F (1,35) = 26.01, *P* < 0.0001], post hoc uncorrected Fisher's LSD multiple comparison test *****P* < 0.0001, **P* < 0.05. Table (*N*) compares time constant, diffusion (*D*), and % mobile receptors. D was calculated using D = 0.25 ($r^2/\tau_{1/2}$), where r refers to the bleach radius and $\tau_{1/2}$ to the time constant (43).

Discussion

Our data show that Parkinson's associated *Lrrk2*^{G2019S} mediates a significant, AMPAR subunit- and SPN-subtype-selective impact on AMPAR composition and cell-surface trafficking in dorsomedial striatum. We found an abnormally increased synaptic and extrasynaptic incorporation of sGluA1, but not sGluA2, in D_1R SPNs, but not in D_2R SPNs. Increased sGluA1-containing AMPARs result in part from their severely impeded internalization that contributes to a saturating ceiling on synapse plasticity by

preventing additional GluA1-AMPAR insertion or recruitment from extrasynaptic pools under activity-dependent conditions. The functional impact is observed in preparations from early postnatal and young adult mice and does not reflect deficient PKA-mediated phosphorylation of GluA1. Together, the data outline a powerful and selective impact on AMPAR trafficking, composition and mobility early in life in the presence of a pathological increase in LRRK2 kinase activity. This, in turn, may contribute to the failure of *Lrrk2*^{G2019S} corticostriatal synapses to express LTP reported previously (9) and could underlie Parkinson-associated impairment in cognitive or other functions that normally rely on intact AMPAR trafficking dynamics.

We found a potent impact of *Lrrk2*^{G2019S} on AMPAR recycling and dynamics by several biochemical and imaging approaches where excessive accumulation of sGluA1 was observed both within and outside of PSD95-defined postsynaptic sites. Our analyses further support that such an increase results from dysfunctional endocytosis, as endogenous GluA1-containing AMPARs showed very little receptor internalization in mutant SPNs compared to WT. Excess sGluA1 levels could also result from more rapid receptor recycling, but this possibility is countered by the absence of SEP-GluA1 fluorescence recovery following photobleaching. The GluA1 internalization defect is likely selective in that transferrin receptor surface expression and internalization were similar between wild type and mutant SPNs, consistent with previous work in iPSC-derived microglia expressing *LRRK2*^{G2019S} (48). Selectivity could be imparted by a targeted impact of LRRK2 on a clathrin-independent pathway (49) or on the juxta-synaptic endocytic zones that preferentially internalize AMPARs (50) and which display distinct clathrin dynamic properties (51).

Several independent measures converge on the outcome that corticostriatally evoked AMPAR-mediated responses in *Lrrk2*^{G2019S} D_1R SPNs are abnormally enriched in synaptic CP-AMPARs, including greater NASPM sensitivity and inwardly rectifying synapses. The biochemical and anatomical data suggest that increased levels of synaptic GluA1-homomers likely correspond to such CP-AMPARs. Consistent with this enrichment, AMPAR:NMDAR ratios were also greater in mutant D_1R SPNs, as would be expected from excessive levels of synaptic sGluA1, although additional changes in NMDARs cannot be ruled out. A previous study (44) failed to observe differences in AMPAR:NMDAR ratios in *Lrrk2*^{G2019S} SPNs, but in that study, recordings were made from subtype-blind SPNs in dorsolateral striatum. Previous studies in WT mice have shown that acquisition of goal-directed learning drives an increase in AMPAR:NMDAR ratios in dorsomedial D_1R SPNs (52). We have shown previously that the *Lrrk2*^{G2019S} mice fail to acquire goal-directed learning (11), suggesting that such behavioral impairment reflects the abnormally larger AMPAR:NMDAR ratios in mutant D_1R SPNs that could occlude further learning-driven increases.

Synaptic delivery of GluA1-AMPARs in response to cLTP (27, 53) failed in *Lrrk2*^{G2019S} SPNs, suggesting these synapses have hit a ceiling of saturation that cannot support further activity-driven insertion of additional GluA1 subunits. In hippocampal CA1 pyramidal neurons, it has been suggested that LTP requires neither specific AMPAR subunits (36) nor insertion of CP-AMPARs (e.g., GluA1) (54), although this is controversial (55) and may represent different mechanisms than those regulating plasticity in nonglutamatergic neurons such as SPNs (56). In the case of *Lrrk2*^{G2019S} SPNs, it may be that receptors cannot easily transit to the PSD or are too firmly anchored. This latter idea is consistent with the failure of GluA2-containing AMPARs to increase at synapses 30 min following a cLTP stimulus as expected, suggesting that in SPNs, AMPARs are not readily exchanged. Additionally, the excess extrasynaptic sGluA1-AMPARs in *Lrrk2*^{G2019S} SPNs do not appear to serve as a reserve pool for rapid synaptic deployment since our FRAP data, which showed significantly decreased recovery and diffusion rates for SEP-GluA1, strongly support that the immobile fraction of sGluA1-AMPARs is enhanced in *Lrrk2*^{G2019S} D_1R SPNs. Alternatively (or additionally), exocytosis or trafficking to synapses may be negatively impacted. A subset of Rab-GTPases, including Rab8 and Rab10 which are typically associated with exocytosis, are validated substrates for LRRK2-mediated phosphorylation (57). Counter to expectation, but similar to what is observed here, hippocampal neurons expressing a dominant negative Rab8, show increased synaptic recruitment of exogenously expressed GluA1 and failed to produce LTP in response to potentiating stimuli (58). LRRK2-phosphorylated Rab8 and Rab10 can also sequester MyosinV proteins (59), which in neurons would be expected to impede the motor protein-dependent transport of AMPARs into spines during LTP (60). Although the basis for the SPN subtype-specific effects is unclear, it may be that relevant LRRK2-targeted effectors such as Rab GTPases are differentially distributed or activated between SPN subtypes.

Our data also suggest that *Lrrk2*^{G2019S} SPNs exert compensatory or adaptive responses to a synaptic excess in sGluA1. The increase in extrasynaptic sGluA1-AMPARs, which are neither readily internalized (Fig. 2) nor mobile (Fig. 4), may be actively excluded from synapses in order to maintain relatively normal synaptic transmission. Consistent with this idea, in mature preparations, the excessive synaptic sGluA1 has a negligible impact on baseline EPSC amplitudes and spine size in *Lrrk2*^{G2019S} SPNs (15, 44). Altered responsiveness appears to emerge when the synapses are challenged, here by a strong potentiating stimulus, which revealed that sGluA1-AMPARs failed to be recruited during induction and sGluA2-AMPAR levels dropped as LTP normally consolidates. The drop in sGluA2-AMPARs may be indicative of a form of postsynaptic LTD that has been described in SPNs (61) and could be consistent with prior work in *Lrrk2*^{G2019S} striatum showing that a normally potentiating stimulus yields instead LTD (9).

Materials and Methods

Animals. Animals were treated in accordance with protocols approved by Mount Sinai's IACUC. Male and female homozygous *Lrrk2*^{G2019S} mice (C57BL/6-Lrrk2tm4.1Arte; 10 to 12 wk old), generated by Eli Lilly labs and characterized previously (16), and age- and strain-matched WT mice were used. All other mice were purchased from Jackson Laboratory. For NASPM experiments, male and female *Lrrk2*$^{G2019S+/-}$ and *Lrrk2*$^{+/+}$ mice heterozygous for *Drd1a*-tdTomato [B6.Cg-Tg(Drd1a-tdTomato)6Calak/J (39)] were used. For FRAP live imaging and superresolution STED imaging, we bred Ai14 mice (B6.Cg-Gt(ROSA)26Sortm14(CAG-tdTomato)Hze/J) ± *Lrrk2*$^{G2019S+/+}$ with mice expressing Cre driven by Drd1a (B6;129-Tg(Drd1-cre)120Mxu/Mmjax).

Culture Preparations. Cortical and striatal neurons (300,000 cells/6 cm dish) were cocultured from E16–18 mice at a ratio of 3:2 as described (62) to ensure normal SPN in vitro development (63). For transfection of pCAG-SEP-GluA1 cDNA (gift of R. Huganir, Johns Hopkins, MD), cocultured neurons were transfected using Lipofectamine 2000 (Invitrogen) at DIV 11–12 according to the manufacturer's recommendations.

Chemical LTP. NMDAR-dependent cLTP was induced in cultured neurons by exposure to glycine as described (28), followed by either surface biotinylation or fixed and immunolabeled.

Electrophysiology. Standard whole-cell patch-clamp recordings from dorsomedially located SPNs were conducted in acute coronal striatal slices to measure NASPM sensitivity, AMPAR:NMDAR ratios, and rectification as described

previously (9, 10, 16). Gabazine (10 μM) was present in all recordings. NASPM sensitivity was assessed by bath-application of the CP-AMPAR antagonist 1-naphthyl acetylspermine (NASPM; Tocris 2756, 200 μM); D-APV (40 μM) was added for rectification experiments.

Imaging. Single confocal optical images of cultured neurons were captured using a Leica SP8 STED 3X microscope with a 63×/1.4 PlanApo oil immersion lens, set to a frame size of 1,024 × 1,024 pixels and 16 bits per pixel. For STED images, a 100× 1.4 STED-HC PlanApo oil immersion lens with an optical zoom of six and a frame size of 1,024 × 1,024 pixels was used to achieve a pixel size of less than 20 nm. Photobleaching experiments were performed live on Zeiss LSM980 Airyscan 2 using the widefield setting. Spines were identified using circular ROIs of diameter 1.2 μm and images were acquired every 2.5 s after bleaching. Nonphotobleached ROIs served as control for fluorescence loss due to imaging.

Statistical Analysis. All data are presented as means ± SEM unless noted otherwise. Specific statistical tests, numbers of mice or cells, and statistical significance are indicated in the figure legends. Statistical analyses were conducted with GraphPad Prism (Version 9.0) software.

Detailed experimental and analysis procedures can be found in *SI Appendix*.

Data, Materials, and Software Availability. RNA data we generated from this work as well as data generated by others are available at GEO [GSE246117 (18), GSE183499 (19), GSE136666 (20)].

ACKNOWLEDGMENTS. This work was supported by R01NS107512 and R21NS130841 from the National Institute of Neurological Disorders and Stroke, the Michael J. Fox Foundation MJFF 022867, the Rainwater Charitable Foundation's 30th Anniversary Tau Leadership Fellowship, and T32-MH087004 from the National Institute of Mental Health. Special thanks to Dr. Richard L. Huganir for providing the SEP-GluA1 construct; Drs. Roger Clem, Yury Garkun, and Ting-Jiun Chen for expert technical advice on electrophysiology experiments; Dr. Abhishek Sahasrabudhe and Romario Thomas for expert technical advice and assistance; and Drs. Almudena Bosch and Bridget Matikainen-Ankney for RNAseq data analysis. Microscopy was performed at the Microscopy Core and Advanced Bioimaging Center at Mount Sinai with assistance from Dr. Nikos Tzavaras and Glenn Doherty for FRAP imaging experiments and from Drs. Shilpa Dilip Kumar and Katarzyna Cialowicz for their guidance with superresolution STED imaging, which utilized a microscope supported with funding from NIH Shared Instrumentation Grant (FAIN: S10OD021838). RNA extraction was performed by the Biorepository and Pathology Core at Mount Sinai and RNAseq was performed at Weill-Cornell Epigenomics Core.

Author affiliations: [a]Nash Family Department of Neuroscience, Icahn School of Medicine at Mount Sinai, New York, NY 10029; [b]Friedman Brain Institute, Icahn School of Medicine at Mount Sinai, New York, NY 10029; and [c]Graduate School of Biomedical Sciences, Icahn School of Medicine at Mount Sinai, New York, NY 10029

1. R. Di Maio *et al.*, LRRK2 activation in idiopathic Parkinson's disease. *Sci. Transl. Med.* **10**, eaar5429 (2018).
2. K. J. Ryan *et al.*, A human microglia-like cellular model for assessing the effects of neurodegenerative disease gene variants. *Sci. Transl. Med.* **9**, eaai7635 (2017).
3. D. Aarsland *et al.*, Parkinson disease-associated cognitive impairment. *Nat. Rev. Dis. Primers* **7**, 47 (2021).
4. A. V. Kravitz, A. C. Kreitzer, Striatal mechanisms underlying movement, reinforcement, and punishment. *Physiology (Bethesda)* **27**, 167–177 (2012).
5. D. M. Lovinger, Neurotransmitter roles in synaptic modulation, plasticity and learning in the dorsal striatum. *Neuropharmacology* **58**, 951–961 (2010).
6. W. Shen, M. Flajolet, P. Greengard, D. J. Surmeier, Dichotomous dopaminergic control of striatal synaptic plasticity. *Science* **321**, 848–851 (2008).
7. A. C. Kreitzer, R. C. Malenka, Striatal plasticity and basal ganglia circuit function. *Neuron* **60**, 543–554 (2008).
8. P. Calabresi, A. Pisani, N. B. Mercuri, G. Bernardi, Long-term potentiation in the striatum is unmasked by removing the voltage-dependent magnesium block of NMDA receptor channels. *Eur. J. Neurosci.* **4**, 929–935 (1992).
9. B. A. Matikainen-Ankney *et al.*, Parkinson's disease-linked LRRK2-G2019S mutation alters synaptic plasticity and promotes resilience to chronic social stress in young adulthood. *J. Neurosci.* **38**, 9700–9711 (2018).
10. A. Tozzi *et al.*, Dopamine D2 receptor activation potently inhibits striatal glutamatergic transmission in a G2019S LRRK2 genetic model of Parkinson's disease. *Neurobiol. Dis.* **118**, 1–8 (2018).
11. A. Hussein, A. Tielemans, M. G. Baxter, D. L. Benson, G. W. Huntley, Cognitive deficits and altered cholinergic innervation in young adult male mice carrying a Parkinson's disease Lrrk2G2019S knockin mutation. *Exp. Neurol.* **355**, 114145 (2022).
12. T. W. Robbins, R. Cools, Cognitive deficits in Parkinson's disease: A cognitive neuroscience perspective. *Mov. Disord.* **29**, 597–607 (2014).
13. A. Perugini, J. Ditterich, A. G. Shaikh, B. J. Knowlton, M. A. Basso, Paradoxical decision-making: A framework for understanding cognition in Parkinson's disease. *Trends Neurosci.* **41**, 512–525 (2018).
14. G. Santangelo *et al.*, Mild cognitive Impairment in newly diagnosed Parkinson's disease: A longitudinal prospective study. *Parkinsonism Relat. Disord.* **21**, 1219–1226 (2015).
15. C. Chen *et al.*, Pathway-specific dysregulation of striatal excitatory synapses by LRRK2 mutations. *Elife* **9**, e58997 (2020).
16. B. A. Matikainen-Ankney *et al.*, Altered development of synapse structure and function in striatum caused by Parkinson's disease-Linked LRRK2-G2019S mutation. *J. Neurosci.* **36**, 7128–7141 (2016).
17. L. Parisiadou *et al.*, LRRK2 regulates synaptogenesis and dopamine receptor activation through modulation of PKA activity. *Nat. Neurosci.* **17**, 367–376 (2014).
18. S. Gupta, B. Matikainen-Ankney, G. W. Huntley, D. L. Benson, Parkinson's-linked LRRK2-G2019S derails AMPAR trafficking, mobility and composition in striatum with cell-type and subunit specificity. GEO Expression Omnibus. https://www.ncbi.nlm.nih.gov/geo/query/acc.cgi?&acc=GSE246117. Deposited 24 October 2023.
19. S. Park, S. Lee, S. Chung, Transcriptome analysis of isogenic Neural stem cell for LRRK2 G2019S mutation. GEO Expression Omnibus. https://www.ncbi.nlm.nih.gov/geo/query/acc.cgi?acc=GSE183499. Accessed 12 March 2023.
20. H. Xicoy, J. F. Brouwers, B. Wieringa, G. J. M. Martens, Explorative combined lipid and transcriptomic profiling of substantia nigra and putamen in Parkinson's disease. *Cells* **9**, 1966 (2020).
21. E. Cerutti *et al.*, Evaluation of sted super-resolution image quality by image correlation spectroscopy (QuICS). *Sci. Rep.* **11**, 20782 (2021).
22. J. W. Lin *et al.*, Distinct molecular mechanisms and divergent endocytotic pathways of AMPA receptor internalization. *Nat. Neurosci.* **3**, 1282–1290 (2000).
23. Q. Zhou, M. Xiao, R. A. Nicoll, Contribution of cytoskeleton to the internalization of AMPA receptors. *Proc. Natl. Acad. Sci. U.S.A.* **98**, 1261–1266 (2001).
24. R. C. Carroll *et al.*, Dynamin-dependent endocytosis of ionotropic glutamate receptors. *Proc. Natl. Acad. Sci. U.S.A.* **96**, 14112–14117 (1999).
25. J. G. Hanley, The regulation of AMPA receptor endocytosis by dynamic protein-protein interactions. *Front. Cell Neurosci.* **12**, 362 (2018).
26. T. Ma *et al.*, Bidirectional and long-lasting control of alcohol-seeking behavior by corticostriatal LTP and LTD. *Nat. Neurosci.* **21**, 373–383 (2018).
27. K. Plant *et al.*, Transient incorporation of native GluR2-lacking AMPA receptors during hippocampal long-term potentiation. *Nat. Neurosci.* **9**, 602–604 (2006).
28. M. Hruska, N. Henderson, S. J. Le Marchand, H. Jafri, M. B. Dalva, Synaptic nanomodules underlie the organization and plasticity of spine synapses. *Nat. Neurosci.* **21**, 671–682 (2018).
29. M. J. Higley, B. L. Sabatini, Competitive regulation of synaptic Ca2+ influx by D2 dopamine and A2A adenosine receptors.. *Nat. Neurosci.* **13**, 958–966 (2010).
30. S. Shi, Y. Hayashi, J. A. Esteban, R. Malinow, Subunit-specific rules governing AMPA receptor trafficking to synapses in hippocampal pyramidal neurons. *Cell* **105**, 331–343 (2001).
31. P. Park *et al.*, Calcium-permeable AMPA receptors mediate the induction of the protein kinase A-dependent component of long-term potentiation in the Hippocampus. *J. Neurosci.* **36**, 622–631 (2016).
32. P. Calabresi *et al.*, Dopamine and cAMP-regulated phosphoprotein 32 kDa controls both striatal long-term depression and long-term potentiation, opposing forms of synaptic plasticity. *J. Neurosci.* **20**, 8443–8451 (2000).
33. S. L. Hawes, F. Gillani, R. C. Evans, E. A. Benkert, K. T. Blackwell, Sensitivity to theta-burst timing permits LTP in dorsal striatal adult brain slice. *J. Neurophysiol.* **110**, 2027–2036 (2013).
34. X. Sun, M. Milovanovic, Y. Zhao, M. E. Wolf, Acute and chronic dopamine receptor stimulation modulates AMPA receptor trafficking in nucleus accumbens neurons cocultured with prefrontal cortex neurons. *J. Neurosci.* **28**, 4216–4230 (2008).
35. D. S. Tukey, E. B. Ziff, Ca2+-permeable AMPA (alpha-amino-3-hydroxy-5-methyl-4-isoxazolepropionic acid) receptors and dopamine D1 receptors regulate GluA1 trafficking in striatal neurons. *J. Biol. Chem.* **288**, 35297–35306 (2013).
36. A. J. Granger, Y. Shi, W. Lu, M. Cerpas, R. A. Nicoll, LTP requires a reserve pool of glutamate receptors independent of subunit type. *Nature* **493**, 495–500 (2013).
37. I. Russo *et al.*, Leucine-rich repeat kinase 2 controls protein kinase A activation state through phosphodiesterase 4. *J. Neuroinflamm.* **15**, 297 (2018).
38. C. R. Ferrario *et al.*, Alterations in AMPA receptor subunits and TARPs in the rat nucleus accumbens related to the formation of Ca^{2+}-permeable AMPA receptors during the incubation of cocaine craving. *Neuropharmacology* **61**, 1141–1151 (2011).
39. K. K. Ade, Y. Wan, M. Chen, B. Gloss, N. Calakos, An improved BAC transgenic fluorescent reporter line for sensitive and specific identification of striatonigral medium spiny neurons. *Front. Syst. Neurosci.* **5**, 32 (2011).
40. M. Koike, M. Iino, S. Ozawa, Blocking effect of 1-naphthyl acetyl spermine on Ca(2+)-permeable AMPA receptors in cultured rat hippocampal neurons. *Neurosci. Res.* **29**, 27–36 (1997).
41. T. A. Verdoorn, N. Burnashev, H. Monyer, P. H. Seeburg, B. Sakmann, Structural determinants of ion flow through recombinant glutamate receptor channels. *Science* **252**, 1715–1718 (1991).
42. R. L. Clem, A. Barth, Pathway-specific trafficking of native AMPARs by in vivo experience. *Neuron* **49**, 663–670 (2006).
43. M. Kang, C. A. Day, A. K. Kenworthy, E. DiBenedetto, Simplified equation to extract diffusion coefficients from confocal FRAP data. *Traffic* **13**, 1589–1600 (2012).
44. M. Volta *et al.*, Initial elevations in glutamate and dopamine neurotransmission decline with age, as does exploratory behavior, in LRRK2 G2019S knock-in mice. *Elife* **6**, e28377 (2017).
45. P. Opazo, D. Choquet, A three-step model for the synaptic recruitment of AMPA receptors. *Mol. Cell Neurosci.* **46**, 1–8 (2011).
46. C. Gao, X. Sun, M. E. Wolf, Activation of D1 dopamine receptors increases surface expression of AMPA receptors and facilitates their synaptic incorporation in cultured hippocampal neurons. *J. Neurochem.* **98**, 1664–1677 (2006).
47. G. Miesenbock, D. A. De Angelis, J. E. Rothman, Visualizing secretion and synaptic transmission with pH-sensitive green fluorescent proteins. *Nature* **394**, 192–195 (1998).

48. A. Mamais *et al.*, Mutations in LRRK2 linked to Parkinson disease sequester Rab8a to damaged lysosomes and regulate transferrin-mediated iron uptake in microglia. *PLoS Biol.* **19**, e3001480 (2021).
49. O. O. Glebov, C. M. Tigaret, J. R. Mellor, J. M. Henley, Clathrin-independent trafficking of AMPA receptors. *J. Neurosci.* **35**, 4830–4836 (2015).
50. J. Lu *et al.*, Postsynaptic positioning of endocytic zones and AMPA receptor cycling by physical coupling of dynamin-3 to Homer. *Neuron* **55**, 874–889 (2007).
51. L. A. Catsburg, M. Westra, A. M. van Schaik, H. D. MacGillavry, Dynamics and nanoscale organization of the postsynaptic endocytic zone at excitatory synapses. *Elife* **11**, e74387 (2022).
52. Q. Shan, M. Ge, M. J. Christie, B. W. Balleine, The acquisition of goal-directed actions generates opposing plasticity in direct and indirect pathways in dorsomedial striatum. *J. Neurosci.* **34**, 9196–9201 (2014).
53. N. Kuhlmann, M. Wagner Valladolid, L. Quesada-Ramírez, M. J. Farrer, A. J. Milnerwood, Chronic and acute manipulation of cortical glutamate transmission induces structural and synaptic changes in co-cultured striatal neurons. *Front. Cell. Neurosci.* **15**, 569031 (2021).
54. H. Adesnik, R. A. Nicoll, Conservation of glutamate receptor 2-containing AMPA receptors during long-term potentiation. *J. Neurosci.* **27**, 4598–4602 (2007).
55. R. L. Huganir, R. A. Nicoll, AMPARs and synaptic plasticity: The last 25 years. *Neuron* **80**, 704–717 (2013).
56. C. Bellone, C. Lüscher, Cocaine triggered AMPA receptor redistribution is reversed in vivo by mGluR-dependent long-term depression. *Nat. Neurosci.* **9**, 636–641 (2006).
57. M. Steger *et al.*, Phosphoproteomics reveals that Parkinson's disease kinase LRRK2 regulates a subset of Rab GTPases. *Elife* **5**, e12813 (2016).
58. T. C. Brown, S. S. Correia, C. N. Petrok, J. A. Esteban, Functional compartmentalization of endosomal trafficking for the synaptic delivery of AMPA receptors during long-term potentiation. *J. Neurosci.* **27**, 13311–13315 (2007).
59. S. S. Khan *et al.*, Pathogenic LRRK2 control of primary cilia and Hedgehog signaling in neurons and astrocytes of mouse brain. *Elife* **10**, e67900 (2021).
60. Z. Wang *et al.*, Myosin Vb mobilizes recycling endosomes and AMPA receptors for postsynaptic plasticity. *Cell* **135**, 535–548 (2008).
61. I. V. Rafalovich *et al.*, Interneuronal nitric oxide signaling mediates post-synaptic long-term depression of striatal glutamatergic synapses. *Cell Rep.* **13**, 1336–1342 (2015).
62. S. Kaech, G. Banker, Culturing hippocampal neurons. *Nat. Protoc.* **1**, 2406–2415 (2006).
63. R. D. Penrod, S. Kourrich, E. Kearney, M. J. Thomas, L. M. Lanier, An embryonic culture system for the investigation of striatal medium spiny neuron dendritic spine development and plasticity. *J. Neurosci. Methods* **200**, 1–13 (2011).